



## Dehydrogenation of methylcyclohexane to toluene over partially reduced silica-supported Pt-Mo catalysts



N. Boufaden <sup>a,\*</sup>, R. Akkari <sup>a</sup>, B. Pawelec <sup>b</sup>, J.L.G. Fierro <sup>b</sup>, M. Said Zina <sup>a</sup>, A. Ghorbel <sup>a</sup>

<sup>a</sup> Laboratoire de Chimie des Matériaux et Catalyse, Département de Chimie, Faculté des Sciences de Tunis, Université de Tunis El Manar, Campus Universitaire Farhat Hached, Rommana 1068, Tunis, Tunisia

<sup>b</sup> Instituto de Catálisis y Petroleoquímica, CSIC, Cantoblanco, 28049 Madrid, Spain

### ARTICLE INFO

#### Article history:

Received 22 February 2016

Received in revised form 12 April 2016

Accepted 13 April 2016

Available online 20 April 2016

#### Keywords:

Hydrogen storage

Methylcyclohexane

Toluene

Pt-Mo catalysts

Silica

### ABSTRACT

A series of bifunctional Pt/Mo(x)-SiO<sub>2</sub> catalysts were investigated in the context of the hydrogen storage using the methylcyclohexane (MCH)-toluene-hydrogen cycle. The performance of partially reduced catalysts for hydrogen production was evaluated in the MCH dehydrogenation reaction carried out in a fixed-bed flow reactor at 673 K and total hydrogen pressure of 2.2 MPa. The catalysts with different acidity and Mo loading (4.1–12.7 wt.%) were prepared by impregnation of the calcined Mo(x)-SiO<sub>2</sub> samples with Pt precursor. The oxide catalyst precursors were characterized by chemical analysis (ICP-AES), N<sub>2</sub> physisorption at 77 K, X-ray diffraction (XRD), Raman spectroscopy and temperature-programmed reduction (H<sub>2</sub>-TPR) techniques whereas the partially reduced samples were characterized by temperature-programmed adsorption of ammonia (TPD-NH<sub>3</sub>), high-resolution transmission electron microscopy (HRTEM) and X-ray photoelectron spectroscopy (XPS). The catalyst having optimized Mo loading (8.0 wt.%) was the most active and its best catalytic performance was attributed to the high dispersion of MoO<sub>2</sub> and Pt<sup>+</sup> phases and its lowest deactivation by coke formation. The activity drop of the catalysts having larger Mo loading (10.6 and 12.7 wt.%) was linked with formation of MoO<sub>x</sub>-Pt core-shell nanoparticles, as confirmed by HRTEM.

© 2016 Elsevier B.V. All rights reserved.

### 1. Introduction

Recently, there has been a great interest in the concept of hydrogen storage in liquid organic hydrocarbons (LOH), such as cyclohexane, methylcyclohexane or decalin [1–4]. In this concept, the hydrogen production from organic hydrocarbons occurs via a catalytic dehydrogenation reaction, being the most favorable, the methylcyclohexane-toluene-hydrogen cycle [5]. In parallel, non-oxidative catalytic dehydrogenation of light alkanes demonstrated to be effective method to produce unsaturated short-chain hydrocarbons. Among different light alkanes, the catalytic dehydrogenation of propane is of particular interest being mixed oxides, such as In<sub>2</sub>O<sub>3</sub>-Ga<sub>2</sub>O<sub>3</sub> [6] and In<sub>2</sub>O<sub>3</sub>-Ga<sub>2</sub>O<sub>3</sub>-Al<sub>2</sub>O<sub>3</sub> [7], promising catalysts to fill the supply-demand gap for propylene.

Since the pioneer works by Sinfelt [5,8], the most suitable catalysts studied for dehydrogenation of methylcyclohexane (MCH) were mainly platinum-based ones, such as Pt/Al<sub>2</sub>O<sub>3</sub> [9–14], Pt/HY [15], Pt/V<sub>2</sub>O<sub>5</sub>, Pt/Y<sub>2</sub>O<sub>3</sub> [4,16,17], and alumina-supported Pt-Re

[16–18]. However, because of the high cost of platinum and its limited terrestrial reserve, the major problem of those catalysts is the high Pt content needed for their preparation (5–10 wt.%). For these reasons, it was essential to find solutions that minimize the catalyst cost while trying to keep the same catalytic performances as monometallic Pt-based ones.

Thus, with the objective to minimize the catalyst cost, some attempts have been made to substitute Pt by non-noble metals, such as Ni [19,20] or Mo [21,22]. In particular, the partially reduced MoO<sub>x</sub> species were found to be effective in the dehydrogenation/isomerization of MCH at varied temperature and pressure conditions [21,22]. This was explained by the presence of Brønsted acidic groups Mo-OH which led to the formation of bifunctional MoO<sub>2</sub>(H<sub>x</sub>)<sub>ac</sub> phase [21,22]. However, as a consequence of the high metal loading, it was difficult to obtain a good dispersion of the active phases on the surface of the support [21]. Indeed, it was reported that the enrichment of the Mo surface decreased or even disappeared in the presence of aromatic hydrocarbons strongly adsorbed on the surface of metal particle [23–25].

Taking into account the good catalytic response of Mo-SiO<sub>2</sub> catalysts prepared by sol-gel method in the reaction of MCH dehydrogenation [21], the promotion of Mo-based catalysts with

\* Corresponding author.

E-mail address: [nesrinebfd@gmail.com](mailto:nesrinebfd@gmail.com) (N. Boufaden).

platinum seems to be a good alternative for reducing the platinum content of the Pt monometallic ones. Since the catalyst dehydrogenation activity increases with the increase of the dispersion of active phases [26], the approach undertaken in this work consists in the preparation of silica-supported bifunctional Pt-Mo catalysts with optimized Mo loading and therefore to enhance the intrinsic activity of partially reduced Mo-SiO<sub>2</sub> catalysts studied previously [21] by their promotion with Pt. In fact, platinum crystallites have the advantage to remove rapidly the hydrogen from the reaction system thanks to their ability to easily dissociate hydrogen atoms, which induces the shift of the chemical equilibrium in favor of the products [27–29]. Moreover, the combination of the ability of Mo atoms to adsorb hydrocarbon species with the rapid dissociation of hydrogen atoms on Pt crystallites [30] may improve both activity and selectivity with respect to monometallic Pt-based catalysts [23–25]. In fact, Pt-Mo catalysts were reported to be active in many hydrotreating reactions such as hydrogenolysis, hydrogenation and dehydrogenation [23–25,31]. In this sense, the large body of the existing work on the dehydrogenation of cycloalkanes allowed to define the catalyst composition and preparation procedures, which are appropriate to minimize the undesired coke deposition on the catalyst surface and also to enhance the stability during on-stream operations [32], which pointes out a possible hydrogen spill-over effects. Indeed, the importance of spilled-over hydrogen in the enlargement of surface area was confirmed for the catalyst prepared by physical mixing of MoO<sub>3</sub> with Pt black [33], as well for the Pt-Mo phases supported on alumina, TiO<sub>2</sub> and Mg-Al [34–36].

The use of a Pt-Mo bimetallic catalyst formulation would create new catalytic sites [30]. In fact, it was found that the reduction of Pt/MoO<sub>3</sub> catalyst with H<sub>2</sub> at 673 K proceeds via the formation of hydrogen molybdenum bronze phase, H<sub>x</sub>MoO<sub>3</sub> [33], which could be responsible for the generation of new catalytic sites as it was reported by Belatet et al. [34]. Concerning the metal function, the enhancement of hexane hydrogenolysis over the Pt-Mo catalyst with respect to monometallic platinum one was explained also in terms of Pt-Mo interaction [31]. Similarly, the enhancement of ethane hydrogenolysis over Mo-Pt/SiO<sub>2</sub> catalysts was explained also as a consequence of a change in the electronic properties of platinum due to its interaction with molybdenum [35].

The silica-supported Mo catalysts studied in this work were prepared by a sol-gel method and not by impregnation because silica exhibits a low amount of basic –OH groups that are able to react with molybdates during impregnation [37]. Indeed, the catalysts prepared by impregnation exhibit a poor dispersion of the active phases on silica substrate which has been considered as the main factor responsible for the low activity [38]. Moreover, the molybdenum oxide structures formed on the support surface after calcination generate more basal planes and lower quantity of defects. This can be disadvantageous as a low fraction of defects inhibit to some extent the reduction of MoO<sub>3</sub> into MoO<sub>2</sub> and after catalyst activation by partial reduction they are the active sites for dehydrogenation of MCH [21]. This is explained by the fact that the kink and step active sites of MoO<sub>2</sub> phase are important for the catalyst activity [39].

In view of the observed discrepancies between the factors influencing the dehydrogenation activities of Pt-Mo catalysts, this work was undertaken with the objective to cover the surface of Mo-SiO<sub>2</sub> catalysts as much as possible by incorporating a large amount of MoO<sub>3</sub> prior to platinum addition. Therefore, the partially-reduced molybdenum oxide phase should be regarded as a support for the platinum active phase, enabling the promoter to be optimally dispersed. Thus, the objective was to elucidate the mutual influence of the modified SiO<sub>2</sub> carrier by MoO<sub>3</sub> and platinum, which could be helpful in increasing our knowledge of this type of catalysts. For the simultaneous control of the textural properties and

homogeneity of Mo species, the Mo-based catalysts were prepared by the sol-gel process. The catalysts were characterized by a variety of physic-chemical techniques in an attempt to explain the relationship between the catalyst performance and structure.

## 2. Experimental part

### 2.1. Catalysts preparation

Four bimetallic Pt/Mo(x)-SiO<sub>2</sub> catalysts, coded hereafter as Pt/Mo(x), where x is the Mo/Si molar percentage, were prepared by wet impregnation of the calcined Mo(x)-SiO<sub>2</sub> samples with an aqueous solution of Pt[(NH<sub>2</sub>)<sub>6</sub>NO<sub>3</sub>]<sub>2</sub> which volume was selected to achieve Pt content of 5 wt.%. In the first step, Mo(x)-SiO<sub>2</sub> samples were prepared through a sol-gel method according to the procedure described previously [21]. Briefly, appropriate amounts of HNO<sub>3</sub> (used as a catalyst for hydrolysis of the silica precursor) and C<sub>2</sub>H<sub>5</sub>OH (solvent; Sigma-Aldrich, 99.8% purity) were mixed in order to adjust the HNO<sub>3</sub>/Si molar ratio at 0.12 with a concentration of silica precursor in EtOH at the value of 0.2 mol L<sup>-1</sup>. Then, the tetraethoxy-silane silica precursor (TEOS, Si(OC<sub>2</sub>H<sub>5</sub>)<sub>4</sub>, Acros, 98% purity) was added dropwise, and then appropriate amount of molybdenum precursor (molybdenum acetylacetone, MoO<sub>2</sub>(C<sub>5</sub>H<sub>7</sub>O<sub>2</sub>)<sub>2</sub>, Merck-Schuchardt) was incorporated in order to obtain Mo\*/100/Si molar ratio of 5, 10, 12 and 15. The mixture was then stirred until gelation while maintaining the temperature at 333 K. The obtained gel was dried in an autoclave under ethanol supercritical conditions (521 K; 6.14 MPa), and then calcined at 773 K under a flux of 30 mL min<sup>-1</sup> of oxygen for 3 h. Finally, the Pt/SiO<sub>2</sub> reference sample (coded hereafter as Pt/SiO<sub>2</sub>) was prepared by wet impregnation of the SiO<sub>2</sub> substrate with an aqueous solution of Pt [(NH<sub>2</sub>)<sub>6</sub>NO<sub>3</sub>]<sub>2</sub>, Alfa Aesar) whose volume was selected to obtain a final Pt content of 5 wt.%. For this catalyst, the bare silica substrate was also prepared by sol-gel method.

### 2.2. Catalyst characterization techniques

The synthesized Pt-Mo silica catalysts prepared by consecutive wet impregnation of calcined Mo-SiO<sub>2</sub> precursors were characterized by chemical analysis (ICP), textural analysis (N<sub>2</sub>-physisorption), X-ray powder diffraction (XRD), H<sub>2</sub>-Temperature-Programmed Reduction (H<sub>2</sub>-TPR), Temperature-Programmed Desorption of ammonia (TPD-NH<sub>3</sub>), High Resolution Transmission Electron Microscopy (HRTEM), Raman and X-ray Photoelectron Spectroscopic (XPS) techniques.

The Pt and Mo loadings of the calcined catalysts were determined by Inductively Coupled Plasma Atomic Emission Spectroscopy (ICP-AES) with a Perkin Elmer Optima 3300DV equipment. The solid samples were first digested for 2 h in a mixture of HF, HCl and HNO<sub>3</sub> carried out in a microwave oven. Then, aliquots of solution were diluted to 50 mL using deionized water.

N<sub>2</sub> adsorption-desorption isotherms were measured at 77 K on a Micromeritics ASAP 2020 physical adsorption analyzer after sample degassing at 473 K for 3 h. The specific surface areas were calculated according to the Brauner-Emmett-Teller (BET) model [40] while the porous distributions were evaluated using the Barrett-Joyner-Halenda (BJH) method [41] applied to the corresponding nitrogen desorption isotherms.

The XRD measurements were performed in the reflection mode within the wide angular range of 4–70° (2θ), using a Siemens D-5000 powder diffractometer operated at 40 kV and 30 mA (Cu-Kα radiation λ = 1.5406 Å) with a scan rate of 0.04° s<sup>-1</sup>. An estimation of the crystalline size was obtained using Scherrer equation.

In order to determine the vibrational and rotational imprint of the samples, Raman spectra were recorded using a Renishaw *in*

Via Raman microscope spectrometer equipped with a laser beam emitting at 532 nm and 100 mW output power. The photons scattered by the sample were dispersed by a 1800 (or 1200) lines/mm grating monochromator and simultaneously collected on a CCD camera; the collection optics was set at 50× objective. The spectral resolution was 1 cm<sup>-1</sup>.

The reducibility of the samples was studied by Temperature-Programmed Reduction with H<sub>2</sub> (TPR-H<sub>2</sub>) using a semi-automatic Micromeritics TPD/TPR 2900 apparatus interfaced to a computer. The samples (0.04 g) were placed in a tubular quartz reactor and swept by a mixture of 5 vol.% H<sub>2</sub> in Ar at a total flow rate of 30 mL min<sup>-1</sup> and then heated at a rate of 15 K min<sup>-1</sup> up to a final temperature of 1073 K.

The acidity of the partially-reduced samples was determined by temperature-programmed desorption (TPD) of ammonia measurements carried out with the same apparatus described for TPR. Before TPD-NH<sub>3</sub> experiment, 0.04 g of each sample was pre-reduced in a quartz reactor at 673 K for 1 h in a flow of 5 vol.% H<sub>2</sub> in Ar mixture. Following this, the sample was cooled to 373 K and ammonia-saturated in a 5% NH<sub>3</sub>/He (Air Liquide) flow (50 mL min<sup>-1</sup>) for 30 min. Then, the sample was subjected to a flow of He (100 mL min<sup>-1</sup>) at 373 K for 15 min to remove any physisorbed NH<sub>3</sub> species from the surface. After catalyst equilibration in a helium flow at 373 K, ammonia was desorbed using a linear heating rate of 10 K min<sup>-1</sup> from 373 K to 873 K. In order to obtain the total acidity of the catalysts, the areas under the curves in the NH<sub>3</sub> desorption profiles were integrated while the Gaussian deconvolution of the peaks allowed a semi-quantitative comparison of the acid strength distribution.

The pre-reduced catalysts were studied by High Resolution Transmission Electronic Microscopy (HRTEM) using a JEM 2100F microscope operating with a 200 kV accelerating voltage and fitted with an INCA X-sight (Oxford Instruments). Before analysis, all the catalysts were crushed into powder, mixed with ethanol and then dispersed in an ultrasonic bath for 10 min. A drop of the suspension was then placed on a carbon-coated Cu grid. To evaluate the particle size distribution, several micrographs of the same sample were analyzed.

X-ray photoelectron spectroscopy was performed in order to reveal the chemical state and the surface composition of calcined, fresh reduced and spent samples. A VG Scientific Ltd., system equipped with a hemispherical electron analyzer and an Mg K $\alpha$  ( $\hbar\nu = 1253.6$  eV) X-ray source. The residual pressure in the ion-pumped analysis chamber was kept below  $9.3 \times 10^{-13}$  MPa during data acquisition. Peak intensities were estimated by calculating the integral of each peak after subtraction of an S-shaped background and fitting the experimental curve to a combination of Gaussian and Lorentzian lines of varying proportion (G/L = 7–30%). The C 1s peak at 284.8 eV (C—C/C—H) was used as the internal standard for determining peak positions.

### 2.3. Methylcyclohexane dehydrogenation

The catalytic performance of the Pt/Mo(x)-SiO<sub>2</sub> catalysts was evaluated in the methylcyclohexane (Spectrophotometric Grade 99%, Sigma-Aldrich) dehydrogenation reaction performed in a bench scale high-pressure laboratory set-up equipped with down-flow fixed bed reactor. In the first step, 0.10 g of the powdered catalyst was dried at 433 K for 30 min with a N<sub>2</sub> flow of 100 mL min<sup>-1</sup>. After that, the catalyst was reduced *in-situ* at 673 K for 3 h with H<sub>2</sub>/N<sub>2</sub> gaseous mixture (molar ratio H<sub>2</sub>:N<sub>2</sub> = 1:5). The optimum temperature for the catalyst reduction was adopted from H<sub>2</sub>-TPR analysis. For activity tests, the MCH was introduced into reactor via a high pressure pump (Knauer HPLC), through the pre-heated line for mixing with H<sub>2</sub> stream. The reaction was carried out at 673 K, 2.2 MPa of total hydrogen pressure, Weight Hourly Space

Velocity (WHSV) of 92.4 h<sup>-1</sup> and H<sub>2</sub>/MCH ratio of 250 L(N) L<sup>-1</sup>. The liquid samples were analyzed using a GC Agilent 6890A equipped with a FID and HP-Innowax column (Crosslinked Polyethylene Glycol) of 30 m length and 0.25 mm of inner diameter and thickness of 0.25 mm (split 300:1). The percent conversion was determined based upon the GC results in terms of mass percent of the products relative to the total mass. The major products resulting from the MCH dehydrogenation were toluene and cyclohexane. Other minor reaction products were isomerization and hydrocracking products: *trans*- and *cis*-1,4-dimethylcyclohexane; *trans*- and *cis*-1,2-dimethylcyclohexane; 2,4-dimethyl-hexane; ethyl-cyclohexane; 1,1-dimethyl-cyclopentane; 1,3-dimethyl-cyclopentane; *trans*-1,2-dimethyl-cyclopentane; *cis*-1,2-dimethyl-cyclopentane, and a low molecular weight paraffins. The selectivity of the catalysts towards these products with respect to the time was determined by:

$$S_i(\%) = c_i \times \sum c_i$$

where c<sub>i</sub> is the molar concentration of product (i) and  $\sum c_i$  is the sum of the molar concentrations of all the products.

A comparison of repeated experiments showed the experiments to be highly reproducible. In addition, carbon balance in all experiments was >99%.

## 3. Results and discussion

### 3.1. Chemical analysis

The chemical compositions of the catalysts determined by ICP-AES technique are summarized in Table 1. It is seen that the real Pt and Mo contents are relatively close to the nominal ones. This is because the solids were prepared via a combination of an acid hydrolytic sol-gel route with an impregnation method. The former method led to the immobilization of molybdenum species through a kinetically controlled hydrolytic polycondensation around the silicon atom leading to the formation of an amorphous silica framework [42]. During the TEOS hydrolysis step, the protonation of the alkoxide group occurs followed by a nucleophilic attack of the water molecule leading to the formation of a pentacoordinate intermediate species. As a consequence of the electron withdrawn from the silicon atom, the silicon atom became more electrophilic and susceptible to be attacked by water, and the leaving group behaved as alkoxide [43]. Then, the polyanion of molybdate might destabilize the positive intermediate species forming molybdenum-containing siloxane species (e.g., Si—O—Mo—O—Si species) [42]. Additionally, some inert Mo polyanions might be formed by their trapping inside the silica during the TEOS hydrolysis and condensation steps. After calcination, the MoO<sub>3</sub>-containing precursors were used for the preparation of binary Pt-Mo catalysts. The ICP-AES analyses (Table 1) also show that the impregnation of the Mo-SiO<sub>2</sub> samples with the platinum solution led to relatively small loss of molybdenum phase.

### 3.2. Textural properties

The textural properties of the catalysts were examined by N<sub>2</sub> adsorption-desorption isotherms at 77 K. Fig. 1(A) shows the N<sub>2</sub> adsorption-desorption isotherms of all samples. The bimetallic catalysts are mesoporous according to the IUPAC nomenclature as they all show type IV isotherms [44]. However, Pt/Mo5, Pt/Mo10 and Pt/Mo12 samples show a unique type H2 hysteresis loop which is usually attributed to different size of pore mouth and pore body i.e. bottle shaped pores [45]. Only Pt/Mo15 sample shows two hysteresis loops, one in relative pressure range of 0.4–0.8 corresponding to type H2 and another one in the relative pressure (P/P<sub>0</sub>)

**Table 1**

Elemental analysis and textural properties of calcined Pt/Mo(x)-SiO<sub>2</sub> samples.

Sample	Mo <sup>a</sup> (wt.%)	Mo <sup>b</sup> (wt.%)	Pt <sup>b</sup> (wt.%)	S <sub>BET</sub> <sup>c</sup> (m <sup>2</sup> g <sup>-1</sup> )	V <sub>total</sub> <sup>c</sup> (cm <sup>3</sup> g <sup>-1</sup> )	Pore diameter <sup>c</sup> (nm)
Pt/Mo5	7	4.1	4.0	458	0.31	3.4
Pt/Mo10	13	8.0	3.8	546	0.32	3.6
Pt/Mo12	15	10.6	3.5	635	0.53	3.8
Pt/Mo15	18	12.7	3.7	489	0.33	3.6

<sup>a</sup> Theoretical (wt.% Pt theoretical is fixed at 5).

<sup>b</sup> As determined by ICP technique.

<sup>c</sup> As determined by N<sub>2</sub> adsorption-desorption isotherms at 77 K.

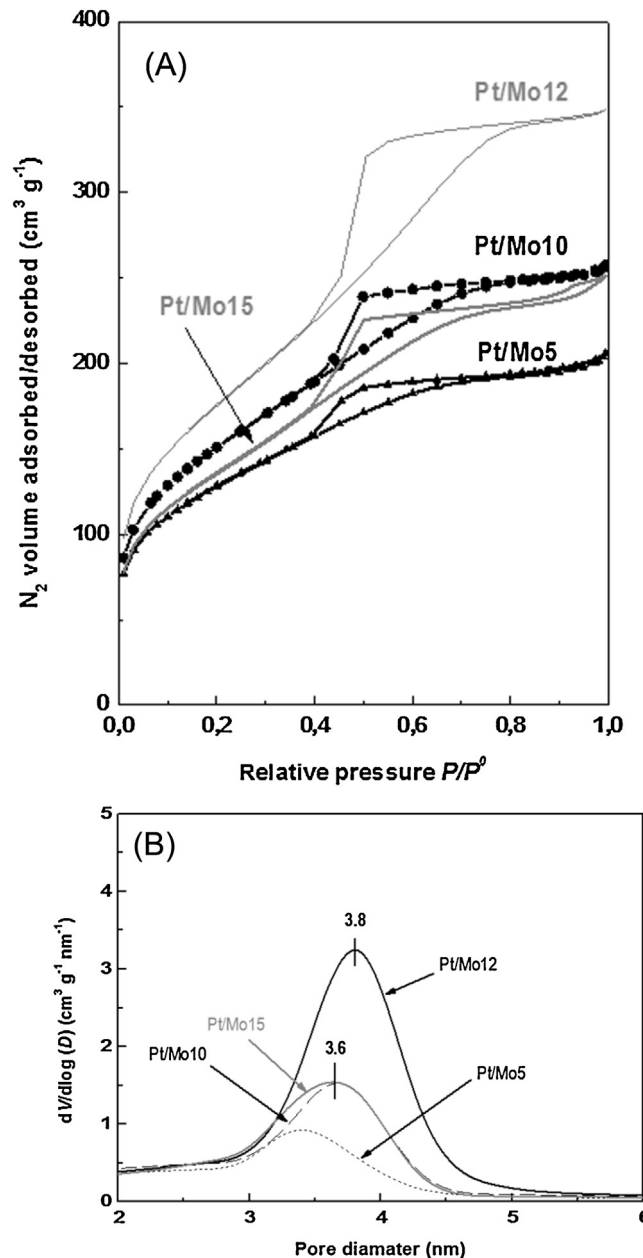


**Fig. 1.** N<sub>2</sub> adsorption-desorption isotherms at 77 K (A), and pore size distribution (B) of calcined Pt/Mo(x)-SiO<sub>2</sub> samples.

of 0.8–1.0 range which belongs to H4 type related to solids consisting of agglomerates or aggregates forming slit-shaped pores [45]. Thus, for samples prepared with low amounts of molybdenum (Mo × 100/Si = 5–12 molar), the shape of N<sub>2</sub> isotherms points out to the formation of the mesopores. On the contrary, the hysteresis loop of the Pt/Mo15 sample suggests the formation of relatively

voluminous Pt and/or Mo aggregates blocking the pore mouths of the support.

The specific surface area (S<sub>BET</sub>), total pore volume and average pore diameter of the prepared solids are listed in Table 1. All samples exhibited a very high specific surface (S<sub>BET</sub>) area (in the range 458–635 m<sup>2</sup> g<sup>-1</sup>). From this table, it is evident that the Pt/Mo(x)-SiO<sub>2</sub> samples show the increase of surface area as the Mo loading is increased: Pt/Mo12 (635 m<sup>2</sup> g<sup>-1</sup>) > Pt/Mo10 (546 m<sup>2</sup> g<sup>-1</sup>) > Pt/Mo15 (489 m<sup>2</sup> g<sup>-1</sup>) > Pt/Mo5 (458 m<sup>2</sup> g<sup>-1</sup>). A similar increase in the specific surface of Pt-MoO<sub>3</sub> catalysts supported on amorphous alumina-silica, Al<sub>2</sub>O<sub>3</sub> and mesoporous silica-alumina was explained in terms of the redispersion of the MoO<sub>3</sub> phase during Pt incorporation by impregnation with platinum salt precursor [37,46,47]. The lower than expected S<sub>BET</sub> of Pt/Mo15 sample could be explained as due to the pore mouths blocking by a large amount of Mo incorporated on the support surface, as suggested by the large drop of total pore volume when going from Pt/Mo12 to Pt/Mo15 sample.

Fig. 1(B) shows the pore size distribution (dV/dlog(D)) for all catalysts, where V is the pore volume (cm<sup>3</sup> g<sup>-1</sup>) and D is the pore diameter (nm). All the catalysts exhibited only one type of pores whose maximum ranges from 3.4 nm to 3.8 nm. The pore volume follows the same trend as S<sub>BET</sub>: the total pore volume increases to a maximum for Pt/Mo12 sample and then decreases for Pt/Mo15 one. The small change of pore diameter from Pt/Mo5 to Pt/Mo12 (Table 1) may indicate of the presence of PtO and MoO<sub>3</sub> crystallites larger than the pore mouths of the silica support which induces the external blocking of the pores without filling them. Meanwhile, the wide curve recorded for the Pt/Mo12 catalyst, would indicate a large pore volume and a remarkable heterogeneity for its porous distribution which fits well with the results reported earlier.

### 3.3. Wide-angle X-ray diffraction (XRD)

The XRD analysis of the samples gives useful information about the crystalline phases present on the support surface. The X-ray diffraction patterns of the four Pt-Mo(x) catalysts are shown in Fig. 2. Pt/Mo5, Pt/Mo10 and Pt/Mo15 catalysts exhibit clear diffraction lines at  $2\theta = 12.7^\circ, 23.3^\circ, 25.7^\circ, 27.3^\circ, 38.9^\circ$  and  $55.7^\circ$  which are attributed to the crystalline orthorhombic  $\alpha$ -MoO<sub>3</sub> phase (JCPDS card 00-005-0508). The MoO<sub>3</sub> crystal size estimated by the Debye-Scherrer equation for the XRD line at  $27.3^\circ 2\theta$  follows the trend: Pt/Mo15 (108.7 nm) > Pt/Mo5 (102.3 nm) > Pt/Mo10 (78.9 nm). On the contrary, Pt/Mo12 did not show clear diffraction peaks belonging to MoO<sub>3</sub> phase indicating that the MoO<sub>3</sub> particles have a crystal size below the detection limit of XRD technique (4 nm) which fits well the information deduced from N<sub>2</sub>-physisorption confirming the highest dispersion of MoO<sub>3</sub> species in this sample. The redispersion of MoO<sub>3</sub> phases during wet impregnation of the calcined Mo5-SiO<sub>2</sub> sample with Pt precursor was also inferred from the N<sub>2</sub> physisorption data (*vide supra*). In addition, all catalysts exhibit 2 diffraction lines at  $2\theta$  of  $40.0^\circ$  and  $46.5^\circ$  corresponding to (111) and (200) reflections, respectively, of the fcc Pt metal phase (JCPDS card

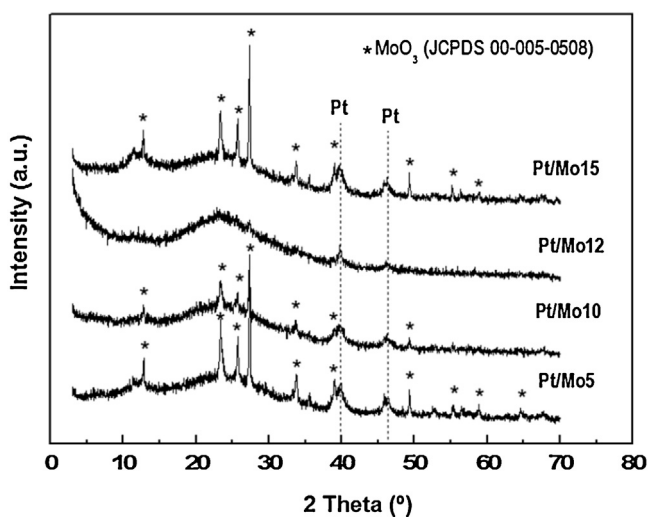


Fig. 2. X-ray diffraction patterns of calcined Pt/Mo( $x$ ) samples.

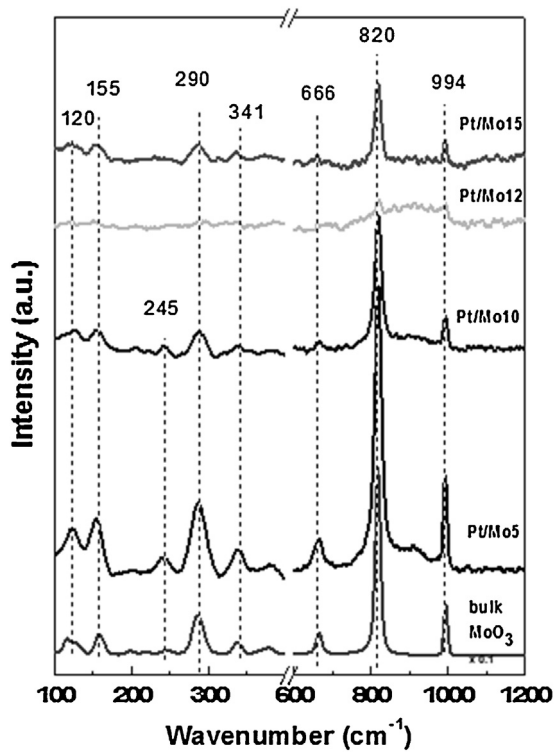


Fig. 3. Raman spectra of calcined Pt/Mo( $x$ )-SiO<sub>2</sub> samples and bulk MoO<sub>3</sub>.

00-001-1194) [48]. In all the patterns, a broad band in the 20°–30° 2θ range characteristic of amorphous silica appeared.

### 3.4. Raman spectroscopy

The nature of platinum and molybdenum species formed after the calcination process was also monitored by Raman spectroscopy. Fig. 3 shows the Raman spectra of Pt/Mo( $x$ ) samples together with bulk MoO<sub>3</sub>. With the exception of Pt/Mo12 sample, the Raman spectra of the different samples show bands similar to that of bulk MoO<sub>3</sub> at 155, 290, 340, 660, 820 and 994 cm<sup>-1</sup>. As reported by Zhen Ou et al. [49], the peak at 155 cm<sup>-1</sup> corresponds to the lattice mode, while the one at 290 cm<sup>-1</sup> represents the bending mode for the double bond (Mo=O) vibration. In addition, the peak at 341 cm<sup>-1</sup> is assigned to Mo<sub>3</sub>—O bending mode while that at 666 cm<sup>-1</sup> can

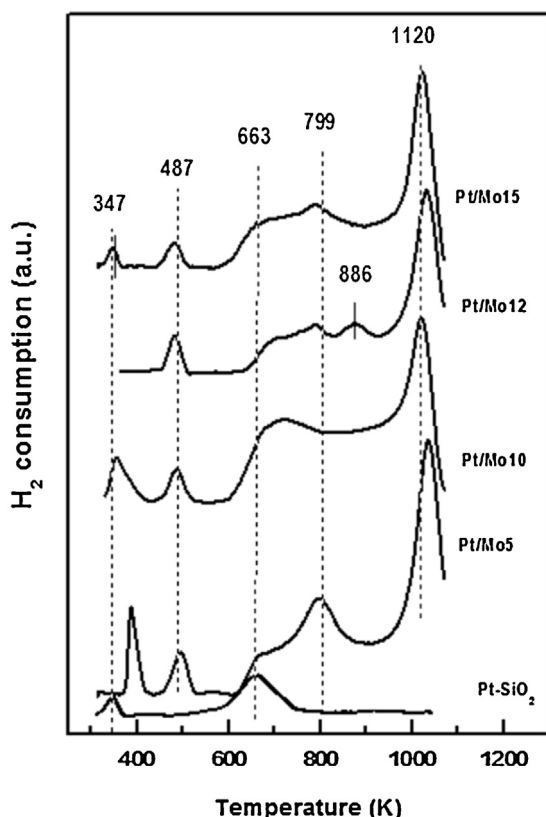
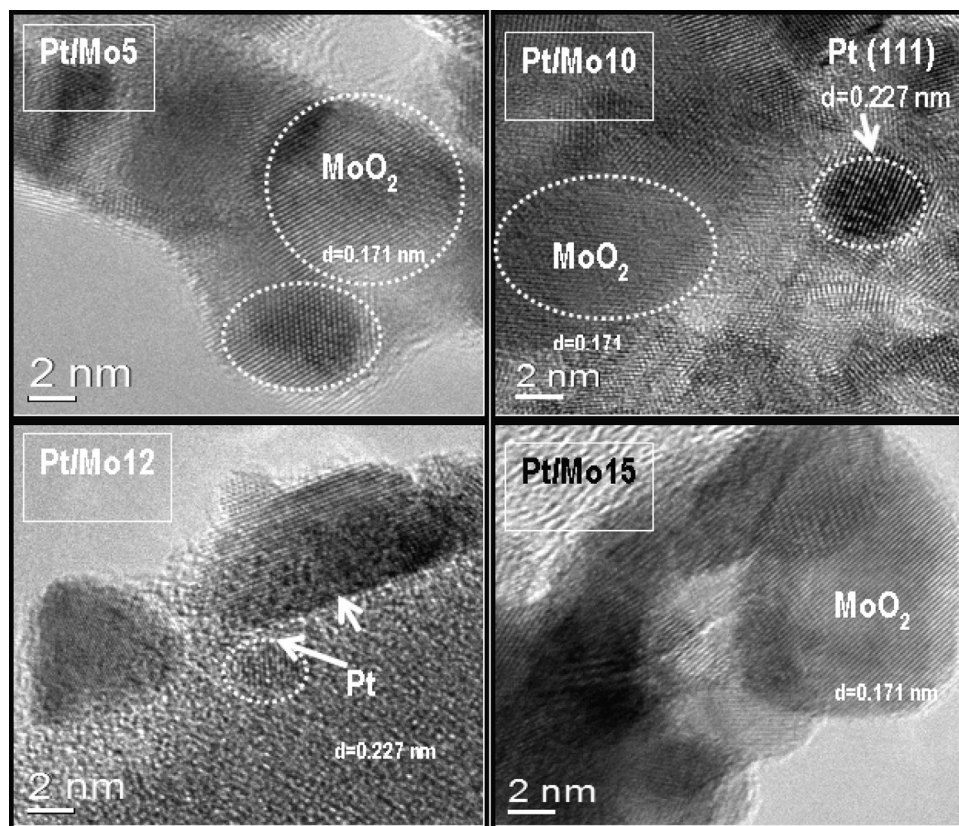


Fig. 4. H<sub>2</sub>-TPR patterns of calcined Pt-SiO<sub>2</sub> and Pt/Mo( $x$ )-SiO<sub>2</sub> samples.

be related to the triply coordinated oxygen (Mo<sub>3</sub>—O) stretching mode. Otherwise, the 820 cm<sup>-1</sup> peak is assigned to the doubly coordinated oxygen (Mo<sub>2</sub>—O) stretching mode, which results from corner-sharing oxygen atoms common to two octahedral. Although the band at 820 cm<sup>-1</sup> is related to the symmetric stretching of the Si—O—Si bonds, the simultaneous presence of a sharp band at 994 cm<sup>-1</sup>, a strong and sharp band 820 cm<sup>-1</sup> and a weak band at 666 cm<sup>-1</sup> agree with bibliography predictions for crystalline MoO<sub>3</sub> nanoparticles [50,51]. Moreover, the position of Raman band at 994 cm<sup>-1</sup> agrees with that reported for symmetric O=Mo=O stretching vibration of di-oxo Mo species [52]. According to such assignments, the band at 994 cm<sup>-1</sup> can be attributed to the stretching vibration mode of such species. The suggested description of the structure of MoO<sub>3</sub> is a layer structure based on the octahedral coordination of Mo atoms (a crystal structure with the symmetry D<sub>2h</sub>) [52].

All these bands are clearly present on the Pt/Mo5 even though almost no peaks were detected in the Raman spectrum of the monometallic Mo5-SiO<sub>2</sub> sample prepared by sol-gel method [21]. The formation of α-MoO<sub>3</sub> crystals for the Pt/Mo5 sample strongly suggests the important changes in the dispersion of Mo species brought about by the consecutive impregnation of the calcined Mo5-SiO<sub>2</sub> precursor with platinum salt precursor. The absence of a significant difference in the terminal Mo-O stretching frequency between bulk MoO<sub>3</sub> and Pt/Mo5 sample suggests the presence of the same types of surface molybdenum oxide species.

Contrary to the Pt/Mo5 catalyst, the two Pt/Mo10 and Pt/Mo15 ones exhibited only two Raman bands (994 cm<sup>-1</sup> and 820 cm<sup>-1</sup>). Taking into account the presence of the most intensive peak of α-MoO<sub>3</sub> species (located at 820 cm<sup>-1</sup>), the formation of MoO<sub>3</sub> crystallites is evident [50,51,53]. Thus, the absence of the band at 666 cm<sup>-1</sup> corresponding to the triply coordinated oxygen could be explained by the re-dispersion of molybdenum species



**Fig. 5.** HRTEM images of partially reduced Pt/Mo( $x$ )-SiO<sub>2</sub> catalysts.

during incorporation of high amounts of platinum which, combined to molybdenum, led to destruction of the large tridimensional Mo<sub>3</sub> species into smaller ones. However, none of these bands are observed on Pt/Mo12 catalyst. Consistently with the N<sub>2</sub> sorption and XRD data (*vide supra*) this observation indicates that, during the incorporation of Pt precursor onto Mo12-SiO<sub>2</sub>, Mo species became redispersed leading the total rearrangement of the large polymolybdates structures and the formation of isolated Mo species [54]. Finally, it is important to note that all Pt/Mo( $x$ ) catalysts did not show bands corresponding to the platinum species suggesting that Pt crystallite size is under the detection limits of this technique.

### 3.5. Temperature-programmed reduction (H<sub>2</sub>-TPR)

In order to obtain information about the eventual relation between the reducibility of the species present on the catalysts and the activity of the partially reduced catalysts in the MCH dehydrogenation, temperature-programmed reduction experiments were carried for selected Pt-Mo( $x$ ) samples together with that of the monometallic Pt/SiO<sub>2</sub> reference. The reduction patterns of analyzed samples are displayed in Fig. 4. It is seen that Pt/SiO<sub>2</sub> sample shows one small reduction peak at 347 K which is usually attributed to the reduction of surface platinum species and another broad one at 663 K related to the reduction of platinum species strongly interacting with the support [55,56].

It is generally known that the reduction pattern of molybdenum based catalysts are rationalized in the light of the stepwise process Mo(VI) → Mo(IV) → Mo(0) [57]. For Pt/Mo( $x$ ) catalysts and despite the similar Pt loading, they showed different TPR profiles (Fig. 4). In fact, for Pt/Mo5 catalyst, three peaks in addition to those recorded for Pt/SiO<sub>2</sub> appeared. Thus, two clear peaks are present at 799 K and 1120 K which would correspond, respectively, to the two reduction steps of the molybdenum oxides. Meanwhile, the peak at

487 K would be attributed to the complete reduction of Pt species having a weak interaction with the support [58]. These three peaks appear on the reduction patterns of all bimetallic catalysts. Remarkably, the peak intensity at 799 K decreased sharply for Pt/Mo12 and Pt/Mo15 catalysts and almost disappeared for Pt/Mo10 one which fits well the findings of Raman spectroscopy. This suggests that the incorporation of platinum would cause the rearrangement of the molybdenum species into isolated ones having smaller sizes than those present in bulk Mo<sub>3</sub> phase which is reported to reduce at higher temperatures [59]. It should be also noted the appearance of a new peak at 886 K on the pattern of Pt/Mo12 sample. Cordero et al. [60] attributed the appearance of more than one peak in the region of 763 K–873 K to the presence of Mo<sub>3</sub> clusters of different size, whereas Jiang et al. [61] explained this in terms of the coexistence of Mo<sub>3</sub> polymolybdates which are easily reduced than crystalline Mo<sub>3</sub>. In the case of Pt/Mo12 catalyst, and in agreement with XRD and Raman results, it can be inferred that impregnation with Pt led to the rearrangement of large Mo<sub>3</sub> polymolybdates into smaller ones as judging by the appearance of the peak at 886 K.

### 3.6. Characterization of partially reduced samples

#### 3.6.1. HRTEM

HRTEM measurements were conducted with the objective to show differences in the active phase dispersion of the catalysts after reduction at 673 K. Fig. 5 shows TEM micrographs of partially-reduced bimetallic catalysts. They reveal ordered crystal structures clearly distinguishable. In fact, the interlayer lattice distance correspond to the [111] diffraction planes typical of the cubic Pt crystalline system ( $d = 0.226$  nm; JCPDS card 00-004-0802) and to MoO<sub>2</sub> crystalline system ( $d = 0.171$  nm; JCPDS card 00-001-0615). Thus, the coexistence of platinum crystallites and MoO<sub>2</sub> clusters was observed in all the samples. This result could then confirm the

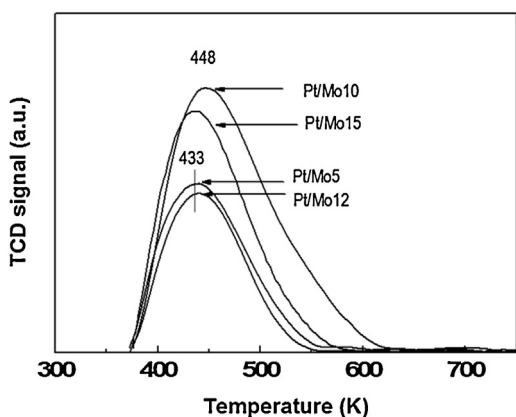


**Fig. 6.** NH<sub>3</sub>-TPD profiles of partially reduced Pt/Mo(x)-SiO<sub>2</sub> catalysts.

presence of MoO<sub>3</sub> crystallites in the oxide precursor prior to partial reduction of the catalysts. The medium particle size was calculated for all bimetallic catalysts for the two types of particles. The statistical calculation of several particles indicated that the medium particle size varies as follows:

- 1.) For Pt particles: Pt/Mo12 (2.21 nm) < Pt/Mo10 (3.8 nm) < Pt/Mo15 (4.29 nm) < Pt/Mo5 (5.3 nm).
- 2.) For MoO<sub>2</sub> particles: Pt/Mo15 (5 nm) < Pt/Mo12 (6.4 nm) Pt/Mo10 (6.8 nm) < Pt/Mo5 (7.1 nm).

These trends indicate that platinum crystallite size is always smaller than that of MoO<sub>2</sub> clusters. In addition, particle sizes confirm the fact that the incorporation of platinum on solids with higher molybdenum loading induced the shrinkage of molybdenum oxide crystallites due to their re-distribution on the surface. It is also important to note that for Pt/Mo5, Pt/Mo12 and Pt/Mo15 catalysts, Pt crystallites are not homogeneously dispersed on MoO<sub>2</sub> while for Pt/Mo10 the number of platinum particles is higher than that of molybdenum oxide, which allows the formation of well dispersed active sites.

### 3.6.2. TPD-NH<sub>3</sub>

The acidity of partially reduced catalysts was evaluated from the temperature-programmed desorption profiles of ammonia (Fig. 6). As seen in Fig. 6, a remarkable difference in the acidic properties is observed among all the samples. Remarkably, for the Pt/Mo10 catalyst, a shift of the peak maxima from 433 K to 448 K and its large and broadened profile suggests the presence of the largest amount of medium strength acid sites. In order to compare the total acidity of the samples, Gaussian functions were used to deconvolute the NH<sub>3</sub> desorption profiles. The total acidity of the samples is listed in Table 2. The total acidity of the partially reduced samples follows the trend: Pt/Mo10 > Pt/Mo15 > Pt/Mo12 ≈ Pt/Mo5. It should be noticed that the superficial silanol groups are known to be weak acid sites. Thus, the deposition of Mo species is expected to give rise to a remarkable increase in the acidity. NH<sub>3</sub>-TPD results show that although the platinum loading is fixed for all the catalysts, the Mo loading could be responsible not only of the difference of the amount of acid sites but also of the acid sites strength and distribution. In fact, it has been reported that the development of acid sites on molybdenum containing catalysts is usually related to the presence of coordinatively unsaturated Mo<sup>6+</sup> species on the surface (Lewis acid sites) [62] and to the presence of hydroxyl groups formed by protonating the bridging Si—O—Mo or terminal Mo=O bonds on the surface (Brønsted acid sites) of the samples [63,64]. Thus, regarding the results provided by the other characterization techniques, it appears that the incorporation of higher

molybdenum loadings results in a decrease of coordinatively unsaturated Mo<sup>6+</sup> but increasing the Si—O—Mo bridges and Mo=O terminals, which may also lead to a modification of the type of the acid sites. For the Pt/Mo10 catalyst, the formation of weak and medium strength acid sites would be beneficial for the reactivity in the target reaction.

### 3.6.3. X-ray photoelectron spectroscopy (XPS)

Before the MCH dehydrogenation, the catalyst activation by partial reduction is necessary. To obtain Mo<sup>4+</sup> species and to avoid total reduction of MoO<sub>3</sub> phase to metallic Mo, the conditions of pre-reduction were soft (673 K for 3 h). XPS experiments allowed evaluating the part of Mo and Pt encountered on the catalysts surface before and after the catalyst activation by reduction. The identification of the Mo and Pt oxidation states by XPS technique is based on the binding energies of the Mo (3d<sub>5/2</sub>, 3d<sub>3/2</sub>) spin-orbit components and the Pt 4f<sub>7/2</sub> core level, respectively. Table 3 lists the binding energies (BE) corresponding to the Mo 3d<sub>5/2</sub> and Pt 4f<sub>7/2</sub> core levels for calcined and partially reduced catalysts. As expected, all calcined and partially reduced samples show binding energies of Mo3d<sub>5/2</sub> level around 232.1 eV (Table 3) corresponding to Mo oxo-species in the highest oxidation state (Mo<sup>6+</sup>) [65]. It is observed that both partially reduced Pt/Mo10 and Pt/Mo12 catalysts show binding energies of Mo 3d<sub>5/2</sub> component shifted to higher values compared to bulk MoO<sub>3</sub> (232.3 vs 231.7 eV) [66] suggesting a stronger interaction between the oxo-molybdenum species and the hydroxyl groups of the silica support and/or an electronic transfer between Pt and Mo particles [30].

The partial reduction of all catalysts under a flow of a H<sub>2</sub>/N<sub>2</sub> gas mixture at 673 K for 3 h led to the formation of Mo<sup>4+</sup> species, as shown by the appearance of a peak at a BE of 229.4 eV (Table 3), since the same BE value was measured by Peterson et al. [67] for the MoO<sub>2</sub>. For Pt/Mo10 catalyst, the reduction conditions were very soft as the major portion of molybdenum species (80%) was still present as Mo<sup>6+</sup> species. The Mo 3d doublet of this sample (not shown here) exhibit broadening which could be explained by the coexistence of several molybdenum species such as Mo<sup>6+</sup>, Mo<sup>4+</sup> and CUS Mo<sup>δ+</sup> surface site ( $0 < \delta < 4$ ) [68]. The partially reduced Pt/Mo15 catalyst was unique showing a very well resolved Mo 3d doublet corresponding to Mo<sup>6+</sup> species. Considering the XRD results (Table 1), this is probably due to formation of large MoO<sub>3</sub> crystals (108.7 nm) on the surface of this sample, which do not reduce under the soft reduction conditions employed.

Concerning the Pt 4f<sub>7/2</sub> core level spectra, it can be noted that oxide precursors of Pt/Mo5, Pt/Mo10 and Pt/Mo15 catalysts exhibit the Pt 4f<sub>7/2</sub> line located at a binding energy of 71.2 eV indicating the formation of metallic Pt species (Table 3). Additionally, the two former samples exhibited a component at binding energy of  $73.4 \pm 0.2$  eV indicating the presence of PtO<sub>x</sub> oxide species [69]. However, after catalyst activation by reduction, all catalysts exhibited only metallic platinum species.

The comparison of the surface Pt/Si and Mo/Si atomic ratios of calcined and pre-reduced samples indicates that the concentration of both Pt and Mo on the support surface after catalyst activation by partial reduction decreases with respect to calcined counterparts (see Table 3). Such a decrease can be caused by the migration of metals into bulk of material during catalyst reduction. The absence of Raman bands of the molybdenum-containing siloxane species, such as a Si—O—Mo—O—Si, indicates that Mo atoms are not embedded in the SiO<sub>2</sub> framework. These results suggest then that both Pt and Mo species are mainly located on the support surface. Noticeably, the most active Pt/Mo10 sample exhibited the most homogeneous Pt and Mo species dispersion among the catalysts studied. For both Pt/Mo12 and Pt/Mo15, the large Pt and Mo species surface exposure determined by XPS is in line with HRTEM information (*vide supra*)

**Table 2**

Cristal size of particles<sup>a</sup> and amount of acid sites<sup>b</sup> of partially reduced Pt/Mo(x)-SiO<sub>2</sub> samples, and amount of carbon on the surface of spent catalysts.<sup>c</sup>

Sample	MoO <sub>2</sub> <sup>a</sup> (nm)	Pt <sup>a</sup> (nm)	Acid sites <sup>b</sup> ( $\mu\text{moles NH}_3 \text{ g}^{-1}$ )	C/Si <sup>c</sup> atomic ratio
Pt/Mo5	7.1	5.3	1.67	0.321
Pt/Mo10	6.8	3.8	3.72	0.167
Pt/Mo12	6.4	2.2	1.64	0.195
Pt/Mo15	5.0	4.3	2.81	0.242

<sup>a</sup> As determined by HRTEM for partially reduced samples.

<sup>b</sup> As determined by TPD-NH<sub>3</sub> for partially reduced samples.

<sup>c</sup> As determined by XPS for spent catalysts.

suggesting the formation of Pt(core)-Mo(shell) structures during catalyst activation.

Finally, the XPS spectra of spent catalysts (data not reported here) confirmed the presence of Pt<sup>0</sup>, MoO<sub>2</sub> (BE at 228.8 eV) and MoO<sub>3</sub> (BE in range 232.1–232.3 eV) phases only. Thus, under the reaction conditions employed ( $T=675 \text{ K } P_{H_2}=2.2 \text{ MPa}$ ), no Mo carbide phase is formed in the course of MCH dehydrogenation over Pt/Mo(x)-SiO<sub>2</sub> catalysts. Contrary to our work, Mo carbide formation was reported during the natural gas conversion over MoO<sub>3</sub> supported on zeolites [51].

### 3.7. Catalytic performance in MCH dehydrogenation

Pt/Mo(x)-SiO<sub>2</sub> catalysts were evaluated in the reaction of MCH dehydrogenation at 673 K and under 2.2 MPa of total H<sub>2</sub> pressure. Before reaction, the catalysts were activated by reduction with gas mixture H<sub>2</sub>:N<sub>2</sub> (1:5) at 673 for 3 h. Fig. 8(A) shows the rates of MCH dehydrogenation with time on stream (TOS) at selected reaction conditions. Regardless of TOS, the dehydrogenation activity of the catalysts follows the trend: Pt/Mo10 > Pt/Mo5 > Pt/Mo12 ≈ Pt/Mo15. Thus, despite the higher Mo loading in the Pt/Mo12 and Pt/Mo15 catalysts, the Pt/Mo10 showed the best catalytic response at the reaction conditions studied. As expected, all binary Pt/Mo(x) catalysts were more active than their monometallic Mo(x)-SiO<sub>2</sub> counterparts [21]. Moreover, considering the effect of Mo loading, the activity of binary samples follows the same trend as those of monometallic Mo(x)-SiO<sub>2</sub> ones [21]. All the catalysts exhibited a good stability during time course of reaction. This is probably because MCH dehydrogenation was carried out at relatively high H<sub>2</sub> pressure of 2.2 MPa, which might diminish the catalyst deactivation by the carbonaceous deposits, known to mainly occur on the acid sites of the catalysts [70]. Noticeably, despite of the largest acidity (Table 2), the spent Pt/Mo10 catalyst exhibited the lowest carbon deposition among the catalysts studied, as deduced from its lowest C/Si atomic ratio (Table 2). Thus, from the information offered in Fig. 7, the lowest coke formation on the Pt/Mo10 catalyst could be tentatively explained by the enhancement of hydrogen dissociation on the well dispersed active sites. Additionally, the dilution effect of MoO<sub>2</sub> might prevent excessive deactivation of the Pt sites of this catalyst. This is because a polymerization type-reaction occurs mainly on continuous Pt sites ( $n>3$ ) which are known to be extensively dehydrogenated surface

species [71]. To gain further insight into this decrease in activity at higher Mo content, in Fig. 8(B) are compared the initial turnover frequencies (TOF), expressed as moles of MCH converted per moles of Pt + Mo (from elemental analysis) and per hour. As seen in this figure, the initial TOF of the catalysts follows the same trend as the specific reaction rates (Pt/Mo10 ≫ Pt/Mo5 ≫ Pt/Mo12 > Pt/Mo15) indicating that the same factors influence on the activity of the catalysts studied.

For all catalysts, the GC-MS analysis of reaction products revealed the presence of toluene as the main product with the appearance of traces of substituted cyclohexanes and cyclopentanes. The yields of toluene and isomerization products at TOS=0 are given in Fig. 8(C). From this figure, it is evident that the Pt/Mo10 catalyst shows the largest yields of toluene and isomerization products among the catalysts studied being yields of toluene 8-times larger than those of the isomerization products. The reaction scheme is shown in Fig. 9. Considering the products detected, the transformation of MCH on silica-supported Pt/Mo(x) catalysts occurs through a bifunctional mechanism. It is known that the isomerization products are formed on acidic sites while toluene is formed on metallic sites of the catalysts after direct dehydrogenation of MCH molecules [4,30]. In fact, the results obtained show clear evidence that the MCH dehydrogenation reaction over Pt/Mo(x)-SiO<sub>2</sub> catalysts occurs mainly on MoO<sub>2</sub>(H<sub>x</sub>) and Pt<sup>0</sup> sites [16,21]. A linear correlation between the initial dehydrogenation activity and the surface Pt<sup>0</sup>/Mo<sup>4+</sup> atomic ratio was confirmed (Fig. 10), suggesting that the activity is proportional to the number of surface Pt and Mo<sup>4+</sup> species. In this sense, for binary Pt-Mo catalysts, it has been suggested that dehydrogenation of MCH has a rate-determining step occurring preferably on Pt sites [53]; unlikely to hydrogenolysis, which was demonstrated to occur much faster on Pt-Mo mixed sites known to be the preferential adsorption sites. The experimental data of the MCH dehydrogenation over Pt catalysts was found to be best fitted using single-site Langmuir-Hinshelwood-Hougen-Watson (LHHW) kinetic mechanism [10,12], which consider the loss of the first hydrogen molecule as the rate determining step and the surface coverage by the methylcyclohexadiene intermediate as negligible.

For all catalysts, a linear correlation between the total amount of acid sites of the samples and the catalyst initial activity was found (Fig. 10) confirming the participation of acid sites in the reaction mechanism. However, the much higher selectivity toward

**Table 3**

Binding energies (eV) of core levels and surface metal atomic ratios of calcined, partially reduced and spent Pt/Mo(x)-SiO<sub>2</sub> samples.

Catalyst	Pretreatment	Mo 3d <sub>5/2</sub> <sup>a</sup>	Pt 4f <sub>7/2</sub> <sup>a</sup>	Mo/Si at	Pt/Si at	Pt <sup>0</sup> /Mo <sup>4+</sup> at
Pt/Mo5	Calcined	232.3	71.2 (55) 73.6 (45)	0.306	0.276	–
	Partially reduced	229.3 (62) 231.1 (38)	71.1	0.075	0.086	1.849
Pt/Mo10	Calcined	232.1	71.2 (46) 73.4 (54)	0.202	0.244	–
	Partially reduced	229.4 (20) 232.3 (80)	71.2	0.116	0.088	3.793
Pt/Mo12	Calcined	232.3	73.1	0.293	0.276	–
	Partially reduced	229.4 (73) 232.3 (27)	71.1	0.183	0.172	1.287
Pt/Mo15	Calcined	232.1	71.2	0.747	0.648	–
	Partially reduced	229.4 (77) 231.2 (23)	71.1	0.227	0.412	2.357

<sup>a</sup> Between parenthesis peak percentages.

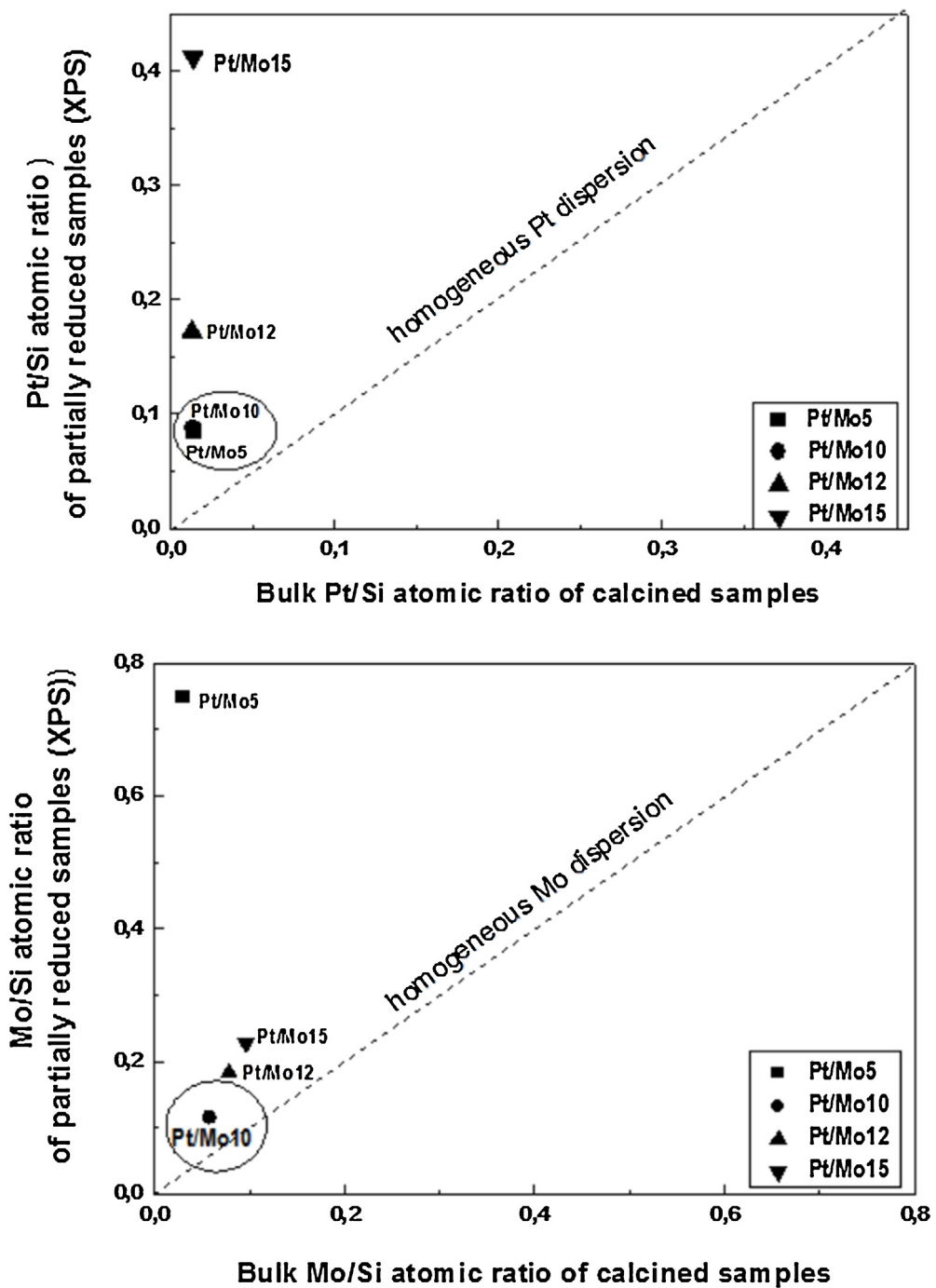


**Fig. 7.** Correlation between XPS Mo/Si and Pt/Si atomic ratios of partially reduced samples and bulk Mo/Si and Pt/Si atomic ratios of calcined samples (from ICP-OES).

dehydrogenation product (toluene) than toward cracking and isomerization products indicates that the metal function dominates over the acidic one. Since a correlation between the Pt/Mo<sup>4+</sup> atomic surface ratio and the initial activity was also found (Fig. 10), it is clear that all catalysts exhibit bifunctional (metallic + acidic) character. In other words, it could be inferred that the observed differences in the initial activity of Pt/Mo(x) catalysts may be associated to the different number of initial Pt and MoO<sub>2</sub> surface species among the samples as well as with their acidity. Considering the metallic function, it is also suggested that platinum addition to Mo(x)-SiO<sub>2</sub> catalysts might enhance the metallic character of the Mo<sub>2-x</sub>(OH)<sub>y</sub> bifunctional system [72], which would facilitate the loss of first H-atom from MCH. However, the structure sensitivity

of MCH dehydrogenation at high H<sub>2</sub> pressure should be different because the difference in the concentrations of the adsorbed carbonaceous deposits generated under different H<sub>2</sub> pressures [73].

On the other hand, both XPS and HRTEM data point out to a strong dependence of the catalyst initial activity on the dispersion of Pt and Mo on the support surface. Thus, the best catalytic activity of Pt/Mo10 catalyst can be explained considering the most homogeneous exposure of their Pt and Mo species on the support surface. In fact, the higher Pt and Mo dispersion can increase the population of the kink and step active sites [39]. This finding is in agreement with Alhumaidan et al. [11], who reported that the increasing in Pt loading in Pt/Al<sub>2</sub>O<sub>3</sub> catalysts negatively influenced Pt dispersion and morphology leading to a decrease in the dehydrogenation

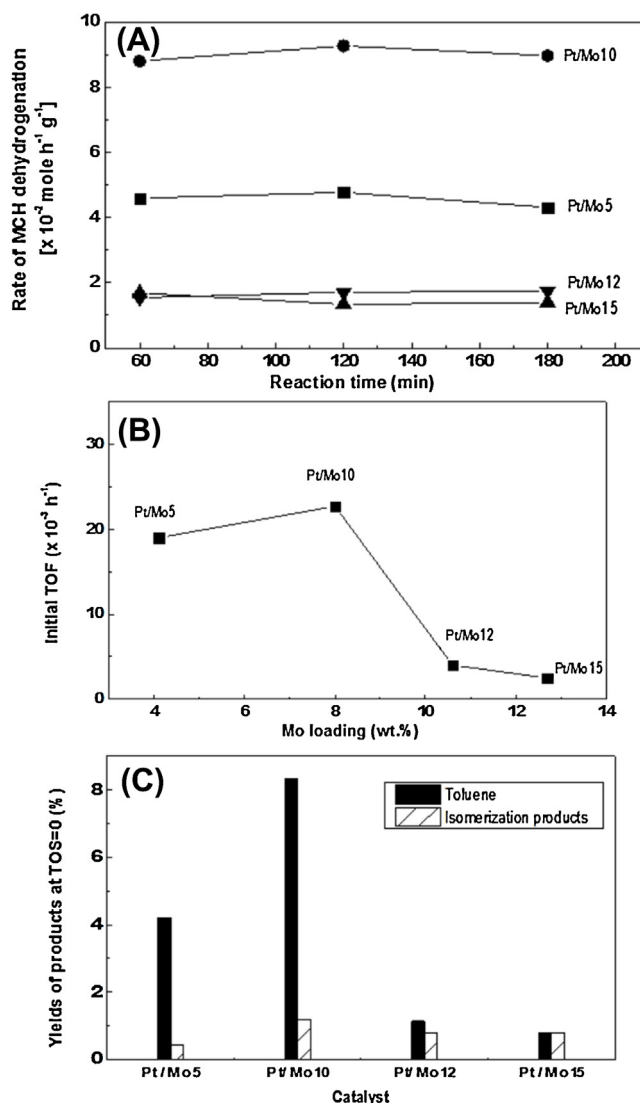


**Fig. 8.** Variation in the activities of partially reduced Pt/Mo( $x$ )- $\text{SiO}_2$  catalysts with time on stream (A), initial TOF (B), and initial yields of products (C) for MCH dehydrogenation reaction ( $T = 673 \text{ K}$ ,  $P_{\text{H}_2} = 2.2 \text{ MPa}$ ). TOF calculated as moles of MCH converted per mole of (Pt + Mo) per second.

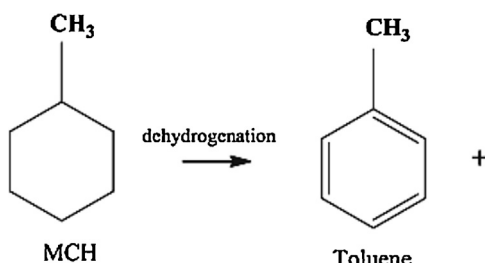


**Fig. 9.** Reaction scheme of the MCH dehydrogenation over partially reduced Pt/Mo( $x$ )- $\text{SiO}_2$  catalysts.

activity. On the contrary to Pt/Mo10, the XPS and HRTEM results suggest that the very low activities of both Pt/Mo12 and Pt/Mo15 catalysts can be caused by the formation of core-shell particles having Pt covered by Mo species (Fig. 5). This fits well the results of Leclercq et al. [23], who reported that the presence of Pt particles on the catalyst surface may be hindered by molybdenum species located on the catalyst surface. Thus, an increase in Mo loading negatively influenced Pt and Mo dispersion and morphology leading

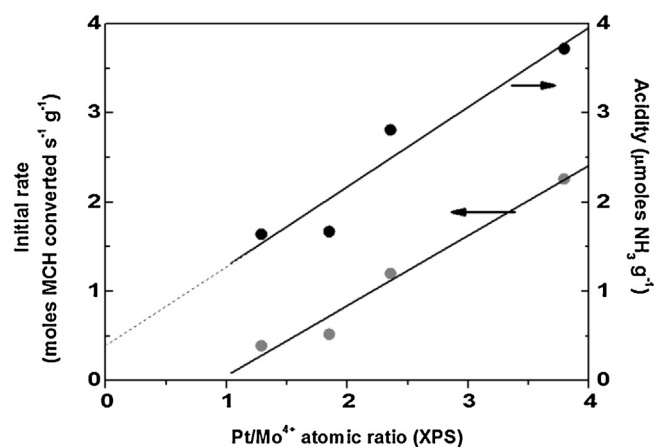


**Fig. 10.** Influence of the acidity (from TPD-NH<sub>3</sub>) and the surface exposure of active phases (expressed as Pt<sup>4+</sup>/Mo<sup>4+</sup> atomic ratio) of the partially reduced samples on the initial catalyst activity.

to lowering the dehydrogenation activity (when  $x > 10$ ). Hence, the best initial activity of the Pt/Mo10 catalyst could be associated with the specific morphology of the MoO<sub>2</sub> and Pt clusters on the silica surface. In this sense, density functional theory calculations (DFT) reported by Gao et al. [74,75] suggested that two adjacent Pt atoms are required for adsorbing an acetylene (H—C=C—H) molecule and a third neighboring Pt one for stabilizing the reacting H-atom during the transformation. However, concerning the geometric requirements needed for MCH dehydrogenation over Pt/Mo-SiO<sub>2</sub> catalysts, our experimental results do not allow us to accurately determine the type of active sites working upon reaction conditions employed. Further reaction kinetic studies and/or DFT calculations should be needed to predict possible geometric requirements for MCH transformation on the clean Pt and MoO<sub>2</sub> surfaces.

#### 4. Conclusions

In this work, the silica-supported partially reduced bimetallic Pt/Mo catalysts were tested in the dehydrogenation reaction of MCH, in the context of the hydrogen storage using methylcyclohexane-toluene-hydrogen cycle. It was concluded that the reaction occurs mainly on MoO<sub>2</sub>(H<sub>x</sub>) and Pt<sup>◦</sup> sites. The best activity and selectivity toward toluene was obtained on the Pt/Mo10 catalyst showing optimized Mo × 100/Si molar ratio of 10. This was linked to its bifunctional character, its homogeneous distribution of Pt<sup>◦</sup> and Mo(VI) on the support surface, and the lowest carbon deposition during time course of the reaction preventing the deactivation on the catalytic reaction. However, larger Mo loadings ( $x = 12$  and 15) induced the formation of MoO<sub>x</sub>-Pt core-shell nanoparticles which caused a drop in the activity of these catalysts.

#### Acknowledgements

Thanks to the Tunisian Ministry of Higher Education, Scientific Research and Information and Communication Technologies for financial support. Financial support by the Community of Madrid (Project S213/MAE-2882) is kindly acknowledged.

#### References

- [1] A. Pradhan, A. Shukla, J. Pande, S. Karmarkar, R. Biniwale, Int. J. Hydrogen Energy 36 (1) (2011) 680–688.
- [2] M. DeLuchi, Int. J. Hydrogen Energy 14 (1989) 81–130.
- [3] F. Alhumaidan, D. Cresswell, A. Garforth, Energy Fuel 25 (2011) 4217–4234.
- [4] F. Alhumaidan, D. Tsakiris, D. Cresswell, A. Garforth, Int. J. Hydrogen Energy 38 (2013) 14010–14026.
- [5] J.H. Sinfelt, J. Mol. Catal. A: Chem. 163 (2000) 123–128.

- [6] S. Tan, L. Briones Gil, N. Subramanian, D.S. Sholl, S. Nair, Ch.W. Jones, J.S. Moore, Y. Liu, R.S. Dixit, J.G. Pendergast, *Appl. Catal. A: Gen.* 498 (2015) 167–175.
- [7] S. Tan, S.-J. Kim, J.S. Moore, Y. Liu, R.S. Dixit, J.G. Pendergast, D.S. Sholl, S. Nair, Ch.W. Jones, *ChemCatChem* 8 (2016) 214–221.
- [8] J.H. Sinfelt, *Adv. Chem. Eng.* 5 (1964) 37–54.
- [9] M. El-Sawi, F. Infortuna, P. Lignola, A. Parmaliana, F. Frusteri, N. Giordano, *Chem. Eng. J.* 42 (3) (1989) 137–144.
- [10] M. Usman, D. Cresswell, A. Garforth, *Ind. Eng. Chem. Res.* 51 (2012) 158–170.
- [11] F. Alhumaidan, D. Cresswell, A. Garforth, *Ind. Eng. Chem. Res.* 49 (2010) 9764–9770.
- [12] F. Alhumaidan, D. Cresswell, A. Garforth, *Ind. Eng. Chem. Res.* 50 (2011) 2509–2522.
- [13] A. Rochedort, F. Le Peltier, J. Boitiau, *J. Catal.* 138 (1992) 482–490.
- [14] W. Doolittle, N. Skoulios, R. Coughlin, *J. Catal.* 107 (2) (1987) 490–502.
- [15] D.K. Cromwell, P.T. Vasudevan, B. Pawelec, J.L.G. Fierro, *Catal. Today* 259 (2015) 119–129.
- [16] A. Shukla, J.V. Pande, R.B. Biniwale, *Int. J. Hydrogen Energy* 37 (2012) 3350–3357.
- [17] A.A. Shukla, P.V. Gosavi, J.V. Pande, V.P. Kumar, K.V.R. Chary, R.B. Biniwale, *Int. J. Hydrogen Energy* 35 (2010) 4020–4026.
- [18] R. Coughlin, K. Kawakami, A. Hasan, *J. Catal.* 88 (1984) 150–162.
- [19] R.B. Biniwale, N. Kariva, M. Ichikawa, *Catal. Lett.* 105 (2005) 83–87.
- [20] S.P. Patil, J.V. Pande, R.B. Biniwale, *Int. J. Hydrogen Energy* 38 (2013) 15233–15241.
- [21] N. Boufaden, R. Akkari, B. Pawelec, J.L.G. Fierro, M. Zina, A. Ghorbel, *Appl. Catal. A: Gen.* 502 (2015) 329–339.
- [22] H. Belatet, H. Al-Kandari, F. Al-Kharafi, F. Garin, A. Katrib, *Appl. Catal. A: Gen.* 318 (2007) 227–233.
- [23] G. Leclercq, S. Pietrzyk, T. Romero, A. El Gharbi, L. Gengembre, J. Grimblot, F. Aissi, M. Guelton, A. Latef, L. Leclercq, *Ind. Eng. Chem. Res.* 36 (1997) 4015–4027.
- [24] G. Leclercq, A. El Gharbi, L. Gengembre, T. Romero, L. Leclercq, S. Pietrzyk, *J. Catal.* 148 (1994) 550–561.
- [25] G. Leclercq, T. Romero, S. Pietrzyk, J. Grimblot, L. Leclercq, *J. Mol. Catal.* 25 (1984) 67–86.
- [26] L.I. Ali, A.-G.A. Ali, S.M. Aboul-Fotouh, A.K. Aboul-Gheit, *Appl. Catal. A: Gen.* 177 (1999) 99–100.
- [27] T.M. Tri, J. Massardier, P. Gallezot, B. Imelik, *J. Catal.* 85 (1984) 244–252.
- [28] N. Kariya, A. Fukuoka, M. Ichikawa, *Appl. Catal. A: Gen.* 233 (2002) 91–102.
- [29] N. Kariya, A. Fukuoka, T. Utagawa, M. Sakuramoto, Y. Goto, M. Ichikawa, *Appl. Catal. A: Gen.* 247 (2003) 247–259.
- [30] K. Jaroszewska, A. Masalska, D. Marek, J.R. Grzechowiak, A. Zemska, *Catal. Today* 223 (2014) 76–86.
- [31] C. Petit, A. Katrib, P. Girard, F. Garin, G. Maire, *J. Mol. Catal.* 85 (1993) 75–95.
- [32] G.C. Bond, *Fundamental and Applied Catalysis (Series)*, Dehydrogenation of Alkanes, Springer, US, 2005, pp. 501–523.
- [33] T. Matsuda, A. Hanai, F. Uchijima, H. Sakagami, N. Takahashi, *Microporous Mesoporous Mater.* 51 (2002) 155–164.
- [34] H. Belatet, H. Al-Kandari, F. Al-Kharafi, A. Katrib, F. Garin, *Appl. Catal. A: Gen.* 275 (2004) 141–147.
- [35] Yu. I. Yermakov, B.N. Kuznetsov, Yu A. Ryndin, *J. Catal.* 42 (1976) 73–78.
- [36] H. Al-Kandari, A.M. Mohamed, F. Al-Kharafi, A. Katrib, *Catal. Commun.* 12 (2011) 1188–1192.
- [37] R. Navarro, B. Pawelec, J.L.G. Fierro, P.T. Vasudevan, *Appl. Catal. A: Gen.* 148 (1996) 23–40.
- [38] G. Muralidhar, F.E. Massoth, J. Shabtai, *J. Catal.* 85 (1984) 44–52.
- [39] S.M. Davis, G.A. Samorjai, *J. Catal.* 65 (1980) 78–83.
- [40] S. Brunauer, P.H. Emmett, E. Teller, *J. Am. Chem. Soc.* 60 (1938) 309–319.
- [41] E.P. Barrett, L.G. Joyner, P.P. Halenda, *J. Am. Chem. Soc.* 73 (1951) 373–380.
- [42] A. Bail, V.C. dos Santos, M. Roque de Freitas, L. Pereira Ramos, W. Herwig Schreiner, G. Pimenta Ricci, K.J. Ciuffi, S. Nakagak, *Appl. Catal. B: Environ.* 130–131 (2013) 314–324.
- [43] A.S. Alfaya, L.T. Kubota, *Quim. Nova* 25 (2002) 835–841.
- [44] K.S.W. Sing, D.H. Everett, R.A.W. Haul, L. Moscou, R.A. Pierotti, J. Rouquerol, T. Siemieniewska, *Pure Appl. Chem.* 57 (1985) 603–619.
- [45] G. Leofanti, M. Padovan, G. Tozzola, B. Venurelli, *Catal. Today* 41 (1998) 207–219.
- [46] Z. Paál, T. Kolta, K. Matusek, J.M. Manoli, C. Potvin, M. Muhler, U. Wild, P. Tetenyi, *Phys. Chem. Chem. Phys.* 3 (2001) 1535–1543.
- [47] D. Gulkova, Y. Yoshimura, Z. Vit, *Appl. Catal. B: Environ.* 87 (2009) 171–180.
- [48] B. Gurau, R. Viswanathan, R.X. Liu, T.J. Lafrenz, K.L. Ley, E.S. Smotkin, E. Reddington, A. Sapienza, B.C. Chan, T.E. Mallouk, S.J. Sarangapani, *Phys. Chem. B* 102 (1998) 9997–10003.
- [49] L. Zhen Ou, J.L. Campbell, D. Yao, W. Włodarski, K. Kalantar-zadeh, *J. Phys. Chem. C* 115 (2011) 10757–10763.
- [50] E.L. Lee, I.E. Wachs, *J. Phys. Chem. C* 111 (2007) 1410–14425.
- [51] J. Gao, Y. Zheng, J.-M. Jehng, I.E. Wachs, S.G. Podkolzin, *Science* 348 (6235) (2015) 686–690.
- [52] S. Chempath, Y. Zhang, A.T. Bell, *J. Phys. Chem. C* 111 (2007) 1291–1298.
- [53] Y. Miao, G. Lu, X. Liu, Y. Guo, Y. Wang, Y. Guo, *J. Mol. Catal. A: Chem.* 306 (2009) 17–22.
- [54] R.D. Roark, S.D. Kohler, J.G. Ekerdt, D.S. Kim, I.E. Wachs, *Catal. Lett.* 16 (1992) 77–83.
- [55] T. Ren-Yuan, W. Rong-An, L. Li-Wu, *Appl. Catal.* 10 (1984) 163–172.
- [56] H. Lieske, G. Lietz, H. Spindler, J. Volter, *J. Catal.* 81 (1983) 8–16.
- [57] A. Galadima, B.M. Ibrahim, *Afr. Sci. J.* 11 (2010) 115–121.
- [58] C. Moran, E. Gonzalez, J. Sanchez, R. Solano, G. Carruyo, A. Moronta, *J. Colloids Interface Sci.* 315 (2007) 164–169.
- [59] J.R. Regalbuto, J.W. Ha, *Catal. Lett.* 29 (1994) 189–207.
- [60] R.L. Cordero, F.J.G. Llambias, A.L. Agudo, *Appl. Catal.* 74 (1991) 125–136.
- [61] H. Jiang, L. Wang, W. Cui, Y. Xu, *Catal. Lett.* 57 (1999) 95–102.
- [62] T. Kataoka, J.A. Dumesic, *J. Catal.* 112 (1988) 66–79.
- [63] L. Vordonis, P.G. Koutsoukos, A. Lycurghiotis, *J. Catal.* 98 (1986) 296–307.
- [64] L. Vordonis, P.G. Koutsoukos, A. Lycurghiotis, *Colloids Surf.* 50 (1990) 353–361.
- [65] Y.V. Plyuto, I.V. Babich, I.V. Plyuto, A.D. Van Langeveld, J.A. Moulijn, *Appl. Surf. Sci.* 119 (1997) 11–18.
- [66] S.O. Grim, L.J. Matienzo, *Inorg. Chem.* 14 (1975) 1014–1018.
- [67] T.A. Paterson, J.C. Carver, D.E. Leyden, D.M. Hercules, *J. Phys.* 80 (1976) 1700–1708.
- [68] D.C. Phillips, S.J. Sawhill, R. Self, M.E. Bussell, *J. Catal.* 207 (2002) 266–273.
- [69] K.S. Kim, N. Winograd, R.E. Davis, *J. Am. Chem. Soc.* 93 (1971) 6296–6297.
- [70] Y. Okada, E. Sasaki, E. Watanabe, S. Hyodo, H. Nishijima, *Int. J. Hydrogen Energy* 31 (2006) 1348–1356.
- [71] J.K.A. Clarke, *Chem. Rev.* 75 (1975) 291–305.
- [72] H. Al-Kandari, A.M. Mohamed, F. Al-Kharafi, M.I. Zaki, A. Katrib, *Appl. Catal. A: Gen.* 417–418 (2012) 298–305.
- [73] I.L.K. Herz, W.D. Gillespie, E.E. Petersen, G.A. Somorjai, *J. Catal.* 67 (1981) 371–386.
- [74] J. Gao, H. Zhao, X. Yang, B.E. Koel, S.G. Podkolzin, *Angew. Chem. Int. Ed.* 53 (9) (2014) 3641–3644.
- [75] J. Gao, H. Zhao, X. Yang, B.E. Koel, S.G. Podkolzin, *ACS Catal.* 3 (6) (2013) 1149–1153.